UCRL-JC-131838
PREPRINT

Magnetic and Thermodynamic Properties of the 3-D Periodic Anderson Lattice Hamiltonian

C. Huscroft
R.T. Scalettar
A.K. McMahan
E.L. Pollock

This paper was prepared for submittal to the
International Conference on Correlation Effects and Materials Properties
Crete, Greece
June 28-July 3, 1998

September 10, 1998

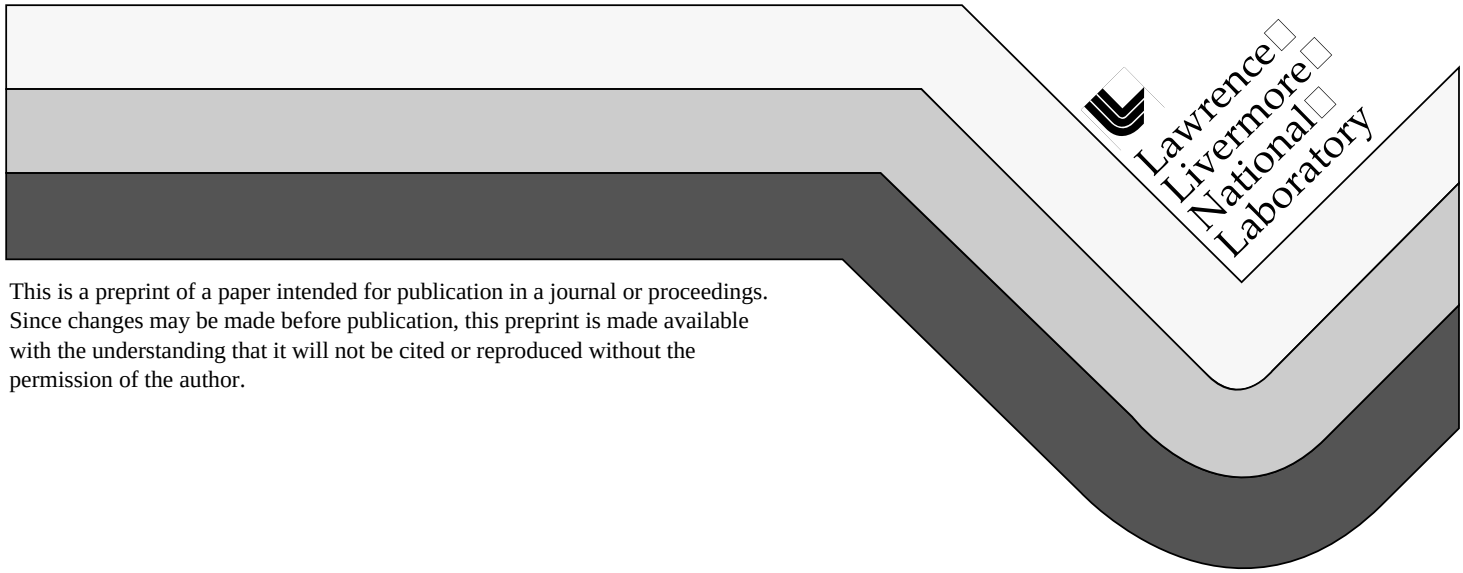

.

MAGNETIC AND THERMODYNAMIC PROPERTIES OF THE 3-D ANDERSON LATTICE HAMILTONIAN

C. Huscroft,[1] R.T. Scalettar,[1] A.K. McMahan,[2] and E.L. Pollock[2]

[1]Physics Department
University of California
Davis, CA 95616

[2] Lawrence Livermore National Laboratory
P. O. Box 808
Livermore, CA 94551

INTRODUCTION

Tight–binding models capture many of the qualitative features of interaction–induced effects in solids. For example, the simplest such model, the single–band Hubbard Hamiltonian, [1] describes the "Mott" insulating phase which occurs in correlated systems, despite the fact that the one electron band is nominally only half–filled, as well as the tendency towards magnetic order. Both phenomena occur in the transition metal oxides. The Periodic Anderson Model (PAM) is a step towards incorporating more complex orbital structure. [2] It contains a pair of orbitals on each site– a delocalized conduction band and a set of highly correlated, localized states. The PAM successfully describes conditions for transitions between antiferromagnetic order of the local moments and phases in which these moments are quenched into singlets paired with conduction electrons. [3] These phenomena are central to heavy fermion systems. [4] The pressure–induced volume collapse in Ce has also been attributed to Kondo–like quenching of the local f moments in this metal, as has been discussed in the context of the impurity Anderson Model. [5]

We will describe Quantum Monte Carlo (QMC) calculations of the magnetic and thermodynamic properties of the PAM in three dimensions. Previous QMC studies have been reported in one and two dimensions. [6,7] A focus of our attention will be on the density of states and the specific heat. The organization of this paper is as follows. We first introduce the PAM and outline some of its properties. Next, a brief presenta-

tion of the Quantum Monte Carlo, Maximum Entropy, and Hartree–Fock methods is given. We then show the equilibrium magnetic properties of the PAM, including the spin correlations between conduction and localized orbitals, and antiferromagnetic correlations in the localized band, before turning to the thermodynamics and the density of states. A concluding section describes connections of this work to the problem of the rare earth volume collapse transitions.

THE ANDERSON LATTICE HAMILTONIAN

The Periodic Anderson Model is,

$$H = -t_{dd} \sum_{\langle ij \rangle \sigma} (d^\dagger_{i\sigma} d_{j\sigma} + d^\dagger_{j\sigma} d_{i\sigma}) - t_{fd} \sum_{\langle ij \rangle \sigma} (d^\dagger_{i\sigma} f_{j\sigma} + f^\dagger_{j\sigma} d_{i\sigma}) + U_f \sum_i (n_{if\uparrow} - \frac{1}{2})(n_{if\downarrow} - \frac{1}{2}) + \epsilon_f \sum_{i\sigma} n_{if\sigma} - \mu \sum_{i\sigma} (n_{if\sigma} + n_{id\sigma}) \,. \quad (1)$$

Here $d^\dagger_{i\sigma}$ and $f^\dagger_{i\sigma}$ represent the creation operators for d and f electrons of spin σ on site i. n_{id} and n_{if} are the total number of up and down spin electrons on the d and f orbitals at lattice site i. t_{dd} and t_{fd} are the intersite valence and f–valence hybridizations, U_f is an on–site repulsion for the f electrons, ϵ_f is the position of the f level, and μ is the chemical potential. The interaction is written in particle–hole symmetric form which has the convenience that at $\mu = \epsilon_f = 0$, both orbitals are precisely half–filled, $n^f_i = n^d_i = 1$, for any choice of t_{dd}, t_{fd}, U_f or temperature T. The choice $\epsilon_f = 0$ is often referred to as the "symmetric" limit of the PAM. We will present results mostly for this case.

Writing the one–body terms in momentum space, the PAM becomes,

$$H = \sum_{k\sigma} \epsilon_k d^\dagger_{k\sigma} d_{k\sigma} + \sum_{k\sigma} V_k (d^\dagger_{k\sigma} f_{k\sigma} + f^\dagger_{k\sigma} d_{k\sigma}) + U_f \sum_i (n_{if\uparrow} - \frac{1}{2})(n_{if\downarrow} - \frac{1}{2}) + \epsilon_f \sum_{k\sigma} n_{kf\sigma} - \mu \sum_{k\sigma} (n_{kf\sigma} + n_{kd\sigma}) \,. \quad (2)$$

In this paper, we will study the properties of the PAM on a simple cubic structure for which,

$$\epsilon_k = -2t_{dd} \left[\cos k_x a + \cos k_y a + \cos k_z a\right] , \quad V_k = -2t_{fd} \left[\cos k_x a + \cos k_y a + \cos k_z a\right] , \quad (3)$$

where a is the lattice constant. Often the PAM is defined with an f–valence hybridization on the same site, leading to a momentum independent V_k. With that choice, even in the non–interacting limit $U_f = 0$ the PAM is an insulator at half–filling owing to the opening of a hybridization gap at the Fermi surface. We believe our choice of near-neighbor intersite hybridization in Eq. 1 is physically well motivated, as strictly onsite one–body terms in the Hamiltonian do not couple different angular momenta. However, it is likely that, while the positions of critical coupling and temperatures are somewhat different, the underlying physics is similar between the two choices.

In numerical solutions of Eq. 2, we have assumed parameters which are roughly characteristic of the rare earths. Specifically, we have taken $t_{dd} = 1$ eV, $U_f = 6$ eV, and considered a range of t_{fd} values. The expression for ϵ_k in Eq. 3 yields a d band of width $12t_{dd}$, and for convenience we shall similarly define an f band width, $W_f = 12t_{fd}$. Parameter calculations show the ratio U_f/W_f has roughly quadratic dependence on atomic volume, due primarily to the variation of t_{fd} with volume. [8]

As we shall describe in detail below, the central issue in numerical and analytic work on the PAM concerns magnetic and thermodynamic properties. As the on–site repulsion U_f increases, double occupancy of the f orbitals is suppressed, and local moments form. This phenomenon is most marked in the symmetric limit where there is on average one electron per f orbital, so that as double occupancy is reduced, each f orbital individually has a single electron and hence a spin. In addition, the Fermi wavevector of the conduction band is $k_F = (1, 1, 1)\pi/a$ which is optimal for staggered order. The central question is then whether the f moments align. In the absence of any direct f–f hybridization, ordering can occur via an indirect RKKY interaction mediated by the conduction electrons. However, there is also a competing tendency. As t_{fd} is increased, d and f electrons can form local singlets, suppressing long range antiferromagnetic order. The local moments are not destroyed through the magnetic transition, instead they remain rather well–formed, but simply lose their coherence.

We will present new QMC results for magnetic order in the three dimensional case. However, we will also focus on the thermodynamics of the transition. We expect that as singlets form, the entropy of the system will be significantly reduced, a phenomenon which might show up as a prominent feature in the energy, specific heat, and free energy. As we will see, observing this is complicated in the symmetric case since one must disentangle the effects of singlet formation from those of magnetic ordering.

CALCULATIONAL TECHNIQUES

Over the last fifteen years, Quantum Monte Carlo techniques have made great progress in simulations of the equilibrium charge, spin, and pairing correlations of two–dimensional correlated electron systems. [9] The usefulness of the approach is that it treats interactions *exactly*. The main limitation is that only finite size systems, typically a few hundred electrons, can be treated. Equivalently, the orbital complexity of models that can be studied is highly constrained. Systems of a few hundred sites or orbitals are, however, an order of magnitude larger than can be studied by exact diagonalization, and large enough so that finite size scaling can often be performed to analyze the thermodynamic limit. A second limitation is that, unless symmetries prevent it, the "sign problem" restricts the accessible parameter range and precludes studies of low temperatures and strong coupling. This, however, does not occur in the symmetric limit of the PAM. In this section we will discuss a particular approach, the determinant QMC algorithm. [10]

We will also describe the "Maximum Entropy" method which has recently been developed to take QMC data and extract *dynamical* information like the density of states, [11] our approach for obtaining the specific heat, and analytic Hartree–Fock calculations with which we will compare our results.

The Determinant Quantum Monte Carlo Method

The central quantity in classical or quantum statistical mechanics is the partition function,

$$Z = \mathrm{Tr} e^{-\beta H}. \tag{4}$$

Just as a trace over any potential energy which is a quadratic form in the position operators can be done in a classical statistical mechanics problem, the trace over a quantum mechanical Hilbert space can be performed analytically for Hamiltonians which are quadratic in the fermion operators. However, the interaction term U_f is quartic, and prevents us from doing the trace. The determinant QMC method is a technique which develops an exact reformulation of the original problem so that only quadratic terms appear.

We can isolate the interaction term by discretizing the inverse temperature, $\beta = L\Delta\tau$. The exponential of the full Hamiltonian $H = K+V$, now has a small parameter in its argument, and we can approximate the full exponential by the product of individual exponentials of the kinetic and potential energies.

$$Z = \mathrm{Tr}[e^{-\Delta\tau H}]^L \approx \mathrm{Tr}[e^{-\Delta\tau K} e^{-\Delta\tau V}]^L. \tag{5}$$

This "Trotter" approximation [12] becomes exact as $\Delta\tau \to 0$. In practice, simulations are conducted at several finite $\Delta\tau$ and the limit then extracted.

The interaction term can then be decoupled by introducing a discrete "Hubbard–Stratonovich" field, [13]

$$e^{-\Delta\tau U(n_{i\uparrow}-1/2)(n_{i\downarrow}-1/2)} = \frac{1}{2} e^{-\Delta\tau U/4} \sum_{S_{i\tau}=\pm 1} e^{\lambda S_{i\tau}(n_{i\uparrow}-n_{i\downarrow})}, \tag{6}$$

with coupling constant λ given by $\cosh(\lambda)=e^{\Delta\tau U/2}$. The Hubbard–Stratonovich field is indexed both by a spatial variable i labeling which of the interaction terms in the Hamiltonian (one for each site) is being decoupled, and an "imaginary time" variable τ which specifies which of the L exponentials of the potential energy is being considered.

The right hand side of Eq. 6 is now quadratic in the fermion operators, so the trace can be performed analytically. The physical content of the procedure is that the set of interacting electrons has been replaced by independent electrons moving in an appropriate fluctuating classical field. The result for the partition function is the product of two determinants, one for each spin species.

$$Z = \sum_{\{S_{i\tau}\}} \det M_\uparrow \det M_\downarrow. \tag{7}$$

These determinants depend on the particular values of the Hubbard–Stratonovich field. The matrices M_σ have dimension the number of spatial sites, N, in the original lattice.

One is really interested in evaluating ratios of traces which represent specific expectation values. Traces which involve additional operators reduce to a similar product of determinants, but with additional matrix elements of the inverse of M. Thus, for example, the equal time fermion Green's function is given by,

$$G_{\uparrow ij} = \langle c_{i\uparrow} c^\dagger_{j\uparrow} \rangle = Z^{-1} \, \mathrm{Tr}[c_{i\uparrow} c^\dagger_{j\uparrow} e^{-\beta H}] = Z^{-1} \sum_{\{S_{i\tau}\}} M^{-1}_{\uparrow ij} \, \mathrm{det} M_\uparrow(S) M_\downarrow(S). \tag{8}$$

Here c is a generic Fermi operator. This takes precisely the form of a classical Monte Carlo problem: If the classical variables $S_{i\tau}$ are generated with a "Boltzmann weight" given by the product of the two determinants, for example with the Metropolis algorithm, the Green's function is given by simply accumulating a simple average of the values of $M^{-1}_{\uparrow ij}$ in the sequence so generated. From G come all quantities of physical interest. Setting $i = j$ allows us to evaluate the occupation $n_{\uparrow i} = 1 - G_{\uparrow ii}$. Making i, j near neighbors determines the kinetic energy. More complicated expectation values of, for example, two particle Green's functions like spin and density correlations can be reduced, via Wick's theorem, to appropriate products of the single particle G.

The Boltzmann weight, the product of the two determinants, is extremely complicated. Specifically, the computation a change in its value, required to do the Monte Carlo, scales as the square of the number of sites in the lattice, N^2. Thus to update all the NL variables requires a computation time which scales as $N^3 L$. It is this fact that limits the size of the simulations that can be performed.

While there are many refinements to this method, [14,15] the above description contains the essence of the methodology.

The Maximum Entropy Method

Above, we described how the determinant QMC method allows the measurement of equal time Green's functions G. It is straightforward, but time consuming, to measure imaginary time displaced Green's functions:

$$G_{\uparrow ij}(\tau) = \langle c_{i\uparrow}(\tau) c^\dagger_{j\uparrow}(0) \rangle = \langle e^{\tau H} c_{i\uparrow} e^{-\tau H} c^\dagger_{j\uparrow} \rangle. \tag{9}$$

Such quantities are needed to measure susceptibilities, where the generalization of the classical fluctuation–dissipation result, $\chi_A = \beta[\langle A^2 \rangle - \langle A \rangle^2]$, to quantum problems is $\chi_A = \int_0^\beta d\tau [\langle A(\tau) A(0) \rangle - \langle A \rangle^2]$.

Unfortunately, one is also very much interested in the Green's functions in *real* time and frequency, but operators like e^{-iHt} are difficult to deal with numerically because of their rapidly fluctuating phases. Thus a crucial task is to relate the imaginary time Green's functions which can be measured in the simulations to real frequency response functions. In principle such relationships are known. For example, the single particle Green's function $G(\mathrm{p},\tau) = \langle c(\mathrm{p},\tau) c^\dagger(\mathrm{p},0) \rangle$, is given by an appropriate convolution of the spectral weight $A(p, \omega)$,

$$G(\mathrm{p},\tau) = \int_{-\infty}^{\infty} d\omega \frac{e^{-\tau\omega}}{1 + e^{-\beta\omega}} A(\mathrm{p},\omega). \tag{10}$$

We want to invert this expression and get the spectral weight from the known Green's function. This inversion, or analytic continuation, is difficult to perform numerically because the kernel is small at large absolute values of the integrand ω. Additionally, the Green's function values obtained from QMC are known only to within statistical error bars. These are small, a tenth of a percent of less typically, but nevertheless because of the ill–conditioned nature of the kernel, significantly different $A(\mathrm{p},\omega)$ will be consistent with the data.

The method of Maximum Entropy [11] circumvents the problem of the ill–defined integrand and noisy Green's function data by utilizing an analytic model of the high energy behavior in combination with a fit to the Green's function data obtained from QMC. The approach has had considerable success for the Hubbard and periodic Anderson Hamiltonians in two dimensions. Here we will apply it to our three dimensional simulations.

Fitting E(T) to Obtain the Specific Heat

The specific heat $C = dE/dT$ can be evaluated from determinant QMC by calculating the energy at two closely spaced temperatures and doing the derivative numerically, or else by measuring $\beta[\langle H^2\rangle - \langle H\rangle^2]$. In practice, both approaches run into serious difficulties. The former has large fluctuations as typically occurs when one takes a numerical derivative of data with statistical errors. The latter approach involves high order Green's functions which are rather noisy, and also some non–trivial considerations concerning the Trotter approximation. [16]

A more promising technique is to take the QMC data for the energy, fit to a reasonable analytic form, and then differentiate the resulting expression. This approach has been applied to the single band Hubbard model in two dimensions to obtain the peaks in C associated with charge and spin fluctuations. [17] Here we will use a similar idea, with, however, a rather different analytic form for the fitting. Specifically, we chose,

$$E(T) = E(0) + \sum_{n=1}^{N} c_n e^{-\beta n \Delta}\,, \tag{11}$$

where Δ and c_n are free parameters. The number of terms N was chosen to be about half of the number of QMC data points fit by this expression. We have verified that other fitting forms give similar results. Various further checks of the procedure come out of the physics, and are described below.

Hartree–Fock Approach

The Hartree–Fock (HF) approach is the simplest analytic technique to incorporate interaction effects. HF takes an interaction term like $U_f n_{if\uparrow} n_{if\downarrow}$ in Eq. 1 and expresses it in the decoupled form $U_f[n_{if\uparrow}\langle n_{if\downarrow}\rangle + \langle n_{if\uparrow}\rangle n_{if\downarrow} - \langle n_{if\uparrow}\rangle\langle n_{if\downarrow}\rangle]$. Typically, one makes an *ansatz* for the form of the expectation values, $\langle n_{i\sigma}\rangle = \rho + \sigma m_u + (-1)^i \sigma m_s$. Here ρ is the electron density per spin, m_u represents a uniform (ferromagnetic) difference in up and down spin occupation, and m_s represents a staggered (antiferromagnetic) difference in occupations. The resulting Hamiltonian is quadratic in the fermion operators and can be diagonalized by going to momentum space. The expectation values ρ, m_u, and m_s are computed self–consistently by filling the resulting single particle levels. One can either compute a global minimum of the free energy by allowing m_u and m_s to take arbitrary values, or restrict them to special values, for example $m_u = m_s$ to get the paramagnetic solution.

HF has a number of well–known drawbacks, some of which are quite disastrous. This is illustrated in Fig. 1 where we show the Néel temperature T_N as a function of the ratio U_f/W_f for a single band Hubbard model corresponding to a simple cubic lattice. [18] The Hamiltonian is like that in Eq. 1 except with a single f orbital, which

has a non–zero f–f hybridization t_{ff}, and an f-band width, $W_f = 12\,t_{ff}$. The on–site repulsion is fixed at $U_f = 6$. T_N is grossly over–estimated at large U_f/W_f. This is a consequence of the fact that the sole magnetic energy scale in HF is set by U_f, the energy for the formation of moments. However, the exchange energy $J = t_{ff}^2/U_f$ is the appropriate scale of the Néel temperature at strong coupling. HF does not know about J and hence at large U_f/W_f has a T_N which goes into the temperature axis at $U_{ff}/4$ instead of going to zero as $1/U_{ff}$. As can be seen in Fig. 1, QMC accurately describes this strong coupling (Heisenberg) limit, the weakly coupled Hartree-Fock limit, and crosses over naturally between these two regimes. [18,19]

There are, of course, many analytic treatments which improve over HF. In subsequent work, we plan on comparing QMC with those approaches. In this manuscript, however, we will focus on the results of QMC, and compare only with HF calculations.

Despite the cautionary message of Fig. 1, when properly interpreted, HF is a useful guide to the effects of interactions. Furthermore, it is worth emphasizing that while HF theory gets T_N qualitatively wrong at strong coupling, one can get at the energy scale J by examining the energy difference between the ferromagnetic and antiferromagnetic HF solutions. This difference does come down as $1/U_{ff}$ at strong coupling. We will exploit this fact later when we suggest further directions for QMC, in particular when suggesting what might occur in the non–symmmetric PAM, where we have yet to carry through detailed QMC simulations.

MAGNETIC CORRELATIONS OF THE SYMMETRIC ANDERSON LATTICE HAMILTONIAN

We first describe the nature of the local moments in the PAM. In Fig. 2 we show the enhancement of the square of the local moment $\mu^2 = \langle (n_{\uparrow i} - n_{\downarrow i})^2 \rangle$ over its value μ_0^2 in the absence of interactions. The x–axis is the ratio of the on–site interaction U_f to the f bandwidth $W_f = 12 t_{fd}$. Moment formation occurs at a temperature set by the "charge fluctuation" energy scale $T/U_f \sim 1/4$ so that in the range shown here, the moment enhancement is temperature independent. Thus, features we will subsequently identify for these temperatures in the specific heat are not caused by entropy associated with moment formation.

As described above, one of the features of the physics of local moments interacting with a delocalized band is the extent to which they form singlets. In the language of the PAM this is measured by the correlation function,

$$c_{fd} = \langle \vec{S}_i^f \cdot \vec{S}_j^d \rangle / [\langle (S_i^f)^2 \rangle \langle (S_i^d)^2 \rangle] \tag{12}$$

Here i and j are near neighbors, and $\vec{S}$ is the vector whose components are $\vec{S}_i = (c_{i\uparrow}^\dagger c_{i\downarrow}^\dagger)\vec{\sigma}\binom{c_{i\uparrow}}{c_{i\downarrow}}$. That is, c_{fd} is just the spin–spin correlation function normalized to the size of the magnetic moment on the two sites. In Fig. 3 we show this quantity for various interaction strengths and temperatures. As the system is cooled at fixed W_f, we see that singlets form. The most rapid variation in c_{fd} is at $U_f/W_f \approx 0.6$.

Measurements of the spin correlations between the f electrons on different sites

$$c_{ff}(l) = \langle \vec{S}_i^f \cdot \vec{S}_{i+l}^f \rangle \tag{13}$$

allow us to determine whether long range antiferromagnetic order is present. In Fig. 4 we show the phase diagram which results from a consideration of the behavior of c_{fd} and c_{ff}. Note, however, that a rigorous treatment of magnetic long range order, such as has been done in two dimensions, [7,20,15] requires simulations on a range of system sizes and an appropriate finite size scaling analysis, Here we have looked only at 4^3 lattices, so our antiferromagnetic phase boundary is only approximate.

THERMODYNAMIC PROPERTIES OF THE SYMMETRIC ANDERSON LATTICE HAMILTONIAN

The results of fitting the energy to the form Eq. 11 for various values of the f–d hybridization are shown in Fig. 5, and, with higher resolution at low temperatures, in Fig. 6. It is useful to compare these results with those of a Hartree–Fock calculation. On the rather coarse energy scale of Fig. 7 it is seen that the antiferromagnetic HF solution appears fairly good. Indeed, it is guaranteed to be exact both at $t_{fd} = 0$ and at $U_f = 0$.

We show the difference between the antiferromagnetic HF and QMC energies in Fig. 8. With the resulting better resolution, we see the two break apart at large t_{fd} (small U_f/W_f) as already suggested by Fig. 7.

The specific heat obtained by differentiating the analytic fits in Fig. 5 is shown in Fig. 9. The points of divergence of the antiferromagnetic HF and QMC energies correlate fairly well with the positions of the sharp peaks in the specific heat of Fig. 9. This is consistent with the notion that HF accurately reflects the charge fluctuation energy scale U_f, but is less good at picking up smaller energy scales associated with more subtle magnetic ordering, whether antiferromagnetism or singlet formation.

The entropy of the system can be computed by evaluating the integrated area,

$$\int_0^\infty dT \frac{C(T)}{T} = \sum_{i=1}^{N} \frac{c_n}{n\Delta} = 4\ln 2 - S_0 \,. \tag{14}$$

Here the term S_0 arises from the fact that on a finite periodic cluster characterized by the dispersion, Eq. 3, the entropy does not go to zero at $T = 0$. For our 4^3 PAM, $S_0 = 0.4332$, as may be directly calculated using HF, since this is a one-body effect. As shown in Fig. 10, we find the sum rule on the total entropy, Eq. 14 is obeyed to within less than 2 percent for $t_{fd} \geq 0.8$, which is a good check both on our QMC simulation and on our fitting procedure for the energy. For smaller t_{fd} the integral instead approaches $3\ln 2 - S_0$, which implies the presence of some missing entropy. That is, for small t_{fd}, the system orders magnetically at temperatures below those accessed in the simulations, $T \geq 0.1 t_{dd}$, which would account for the missing $\ln 2$ in the entropy.

DYNAMIC PROPERTIES OF THE SYMMETRIC ANDERSON LATTICE HAMILTONIAN– THE DENSITY OF STATES

The evolution of the f density of states with changing f–valence hybridization is given in Fig. 11. For $t_{fd} = 0$ we have completely isolated localized sites, and therefore expect to have two delta function peaks at $\pm U_f/2 = \pm 3$. That is, we have two infinitely narrow Mott bands, separated by a Mott gap U_f. Our choice of the form of the interaction places these symmetrically about $\omega = 0$. As t_{fd} is made non–zero, the f electrons increasingly hybridize with the conduction band and their density of states widens. Eventually a structure appears which has both broad remnants of the Mott bands, but also Kondo resonance peaks near $\omega = 0$.

It is also interesting to examine the temperature dependence of the f density of states at fixed t_{fd}. We show this in Fig. 12. At high temperatures there is only a pair of Mott peaks associated with charge fluctuations on the f orbital. As T is lowered, sharp Kondo resonances split off of these broad structures. The suppression of the f density of states at $\omega = 0$ which separates the sharp peaks can arise either as a result of the development of an antiferromagnetic gap, or as a Kondo gap associated with the energy required to break a singlet pair.

The Kondo resonance in $N_f(\omega)$ is a further signature of singlet formation in the PAM. It develops at a temperature which coincides with that for which the static spin–spin correlation function c_{fd} shows antiferromagnetic correlations are developing between the f and d electron spins. Similarly, the resonance develops at a temperature in rough coincidence with the peak in the specific heat shown in Fig. 9. However, because in the same temperature range antiferromagnetic correlations among the f moments are also developing, we cannot as yet unambiguously attribute the thermodynamic signature to singlet formation.

We have seen that the Hartree–Fock technique overestimates T_N and also fails to capture the thermodynamics of spin ordering at low temperatures $T \sim J$. It is interesting to ask what HF theory predicts for the density of states. The answer is that HF theory can describe the strong coupling case where two Mott bands exist at $\omega = \pm U_f/2$ as well as the weak coupling metallic limit where a single broad feature in $N_f(\omega)$ is centered about $\omega = 0$. However, it cannot correctly capture the intermediate case where a Kondo resonance develops.

CONCLUSIONS

The periodic Anderson Hamiltonian is the fundamental model of interacting local bands and delocalized conduction electrons. It contains the essential competition between the tendency towards singlet formation of the local electron and conduction electron spin, and antiferromagnetic order in the local band, and has been used as a qualitative model of heavy fermion and other systems. Here we have presented new results for its magnetic and thermodynamic properties in three dimensions.

In this concluding section of the manuscript we turn to a more specialized application of the PAM, namely to the problem of volume collapse transition in rare earth systems.

Several Lanthanides exhibit phase transitions under pressure characterized by abnormally large volume changes (14% for Cerium and 9% for Praseodymium), as has recently been reviewed. [8] The physical mechanisms responsible for these transitions

have been debated since discovery of the Cerium phenomenon over 50 years ago. Currently, the two main viable conjectures [21] are a Mott transition of the 4f electrons accompanied by magnetic ordering, [22] and a "Kondo volume collapse" due to rapid change in the $4f$–valence electron coupling. [5] While some estimates of the free energy changes in the two scenarios have been made which indicate that the size may be in the right ball–park to drive the transition, it is useful to have exact treatments of specific correlated electron Hamiltonians to test the ideas more quantitatively.

We have demonstrated sharp thermodynamic signatures in both the low-temperature specific heat and in the t_{fd} (or atomic volume) dependence of the total energy for the PAM, and correlated these features with structure in the f electron density of states. These features are not reproduced in simpler Hartree–Fock calculations. The former is absent also in more sophisticated approaches [23] we have attempted, where, however, there is some suggestion of similar t_{fd} dependence in the total energy. Whether these effects are sufficiently large, and sufficiently abrupt, to drive the volume collapse transitions is still unclear. In the symmetric limit that we have studied to date, the situation is also complicated by the presence of antiferromagnetic ordering in the model.

Hartree–Fock calculations, despite their weaknesses, can give us some qualitative insight into the probable effect of going to the non–symmetric limit on the antiferromagnetic ordering, either by shifting f level ϵ_f away from zero or else by adjusting the chemical potential μ to go off half–filling. In Fig. 13 we show the results of HF calculations in the case of a shifted f level. We see that the tendency to antiferromagnetic order is reduced. We plan, therefore, to carry out simulations in the non–symmetric case where we can be more sure that the thermodynamic signatures are not associated with long range magnetic order.

It remains to be established that this transition in the PAM occurs in a reasonable place on the experimental phase diagram. This requires making a determination of the volume dependence of the PAM parameters through, for example, a connection to LDA calculations. [8] This connection involves either developing a mapping of the full, many f and conduction band structure to the simpler PAM, or else QMC simulations of more complicated multi–band models.

ACKNOWLEDGEMENTS

This work was performed under the auspices of the U.S. Department of Energy by Lawrence Livermore National Laboratory under Contract No. W-7405-Eng-48, and the Accelerated Strategic Computing Initiative. We are also grateful to the hospitality of the Lawrence Livermore National Laboratory Materials Research Institute, where part of this work was performed.

REFERENCES

[1] J. Hubbard, Proc. R. Soc. London **A276**, 238 (1963); *ibid* **A277**, 237 (1964); *ibid* **A281**, 401 (1964). For a collection of recent papers, see, "The Hubbard Model," A. Montorsi (ed), World Scientific, 1992.

[2] P.W. Anderson, Phys. Rev. **124**, 41 (1961).

[3] P. Fulde, J. Keller, and G. Zwicknagel, Solid State Physics **41**, 1 (1988); D.W. Hess, P.S. Riseborough, and J.L. Smith, Ency. Appl. Phys., **7**, 435 (1993).

[4] G.R. Stewart, Rev. Mod. Phys. **56**, 755 (1984); P.A. Lee, T.M. Rice, J.W. Serene, L.J. Sham, and J.W. Wilkins, Comm. on Cond. Mat. Phys. **12**, 99 (1986).

[5] J.W. Allen and R.M. Martin, Phys. Rev. Lett. **49** 1106 (1982); J.W. Allen and L.Z. Liu, Phys. Rev. **B46**, 5047 (1992); M. Lavagna, C. Lacroix, and M. Cyrot, Phys. Lett. **90A**, 210 (1982); J. Phys. F **13**, 1008 (1983).

[6] R.M. Fye, Phys. Rev. **B41**, 2490 (1990).

[7] M. Vekic, J.W. Cannon, D.J. Scalapino, R.T. Scalettar, and R.L. Sugar, Phys. Rev. Lett. **74**, 2367 (1995).

[8] A. McMahan, C. Huscroft, R.T. Scalettar, and E.L. Pollock, Journal of Computer-Aided Materials Design, to appear.

[9] For reviews see: D.J. Scalapino, in *Proceedings of the International School of Physics* (July 1992), R. A. Broglia and J.R. Schrieffer, eds. (North-Holland, New York, 1994); and E. Dagotto, Rev. Mod. Phys. **66**, 763 (1994).

[10] R. Blankenbecler, D.J. Scalapino, and R.L. Sugar, Phys. Rev. **D24**, 2278 (1981).

[11] M. Jarrell and J.E. Gubernatis, Phys. Rep. **269**, 135 (1996).

[12] H. F. Trotter, Proc. Am. Math. Soc. **10**, 545 (1959); M. Suzuki, Comm. Math. Phys. **51**, 183 (1976).

[13] R.L. Stratonovich, Dokl. Akad. Nauk. SSSR **115**, 1097 (1957); J.E. Hirsch, Phys. Rev. **B31**, 4403 (1985).

[14] G. Sugiyama and S.E. Koonin, Ann. Phys. **168**, 1 (1986); S. Sorella, S. Baroni, R. Car, and M. Parrinello, Europhys. Lett. **8**, 663 (1989); S. Sorella, E. Tosatti, S. Baroni, R. Car, and M. Parrinello, Int. J. Mod. Phys. **B1**, 993 (1989).

[15] S.R. White, D.J. Scalapino, R.L. Sugar, E.Y. Loh, Jr., J.E. Gubernatis, and R.T. Scalettar, Phys. Rev. **B40**, 506 (1989).

[16] R.M. Fye and R.T. Scalettar, Phys. Rev. **B36**, 3833 (1987).

[17] D. Duffy and A. Moreo, Phys. Rev. **B55**, 12918 (1997).

[18] R.T. Scalettar, D.J. Scalapino, R.L. Sugar, and D. Toussaint, Phys. Rev. **B39**, 4711 (1989)

[19] The Néel temperature for the single band Hubbard Hamiltonian has also been

computed within "dynamical mean field theory." The results are in much better agreement with QMC. In particular, the strong–coupling Heisenberg limit is correctly picked out.

[20] J.E. Hirsch and S. Tang, Phys. Rev. Lett. **62**,591 (1989).

[21] Interestingly, there have been some recent suggestions, that in fact the two mechanisms may be related, with the sharp quasiparticle peak in the single band Hubbard model playing a similar role to that of the Kondo resonance in a multi–band model.

[22] B. Johansson, Philos. Mag. **30**, 30 (1974).

[23] M.M. Steiner, R.C. Albers, D.J. Scalapino, and L.J. Sham, Phys. Rev. **B43**, 1637 (1991).

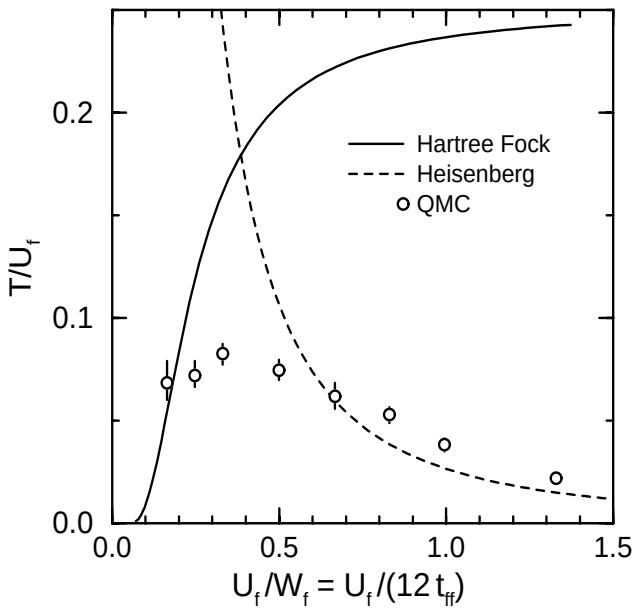

FIG. 1. The Néel temperature of the single band Hubbard model as calculated within Hartree–Fock (solid line), Heisenberg (dashed line), and Quantum Monte Carlo simulations (open circles).

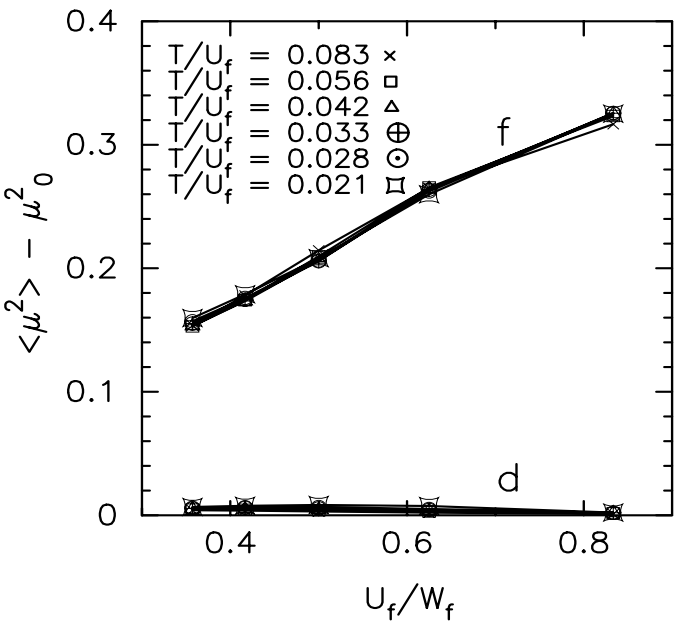

FIG. 2. Enhancement of the local moments on the f and d orbitals over their non–interacting values. Local moment formation occurs at a relatively high temperature, so that the results shown here are independent of T.

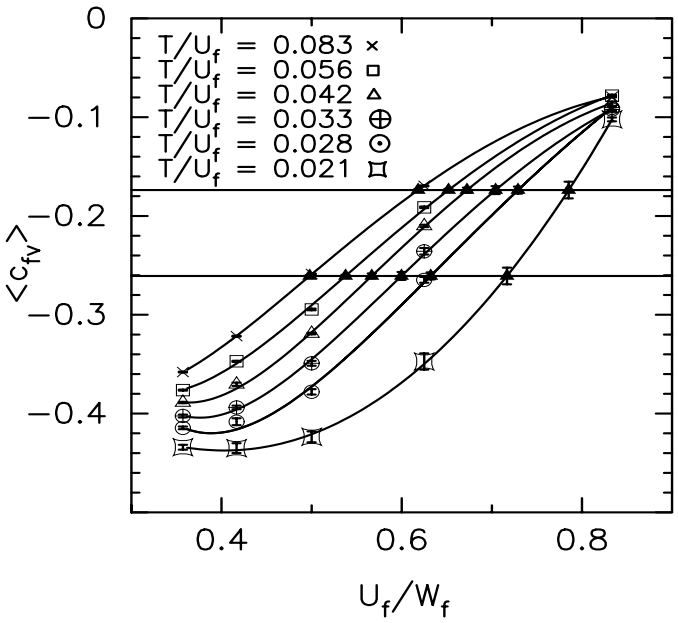

FIG. 3. The spin correlations between the d and f electron moments is shown as a function of U_f/W_f for different temperature values. The horizontal lines give an approximate range for the cross–over to a singlet phase.

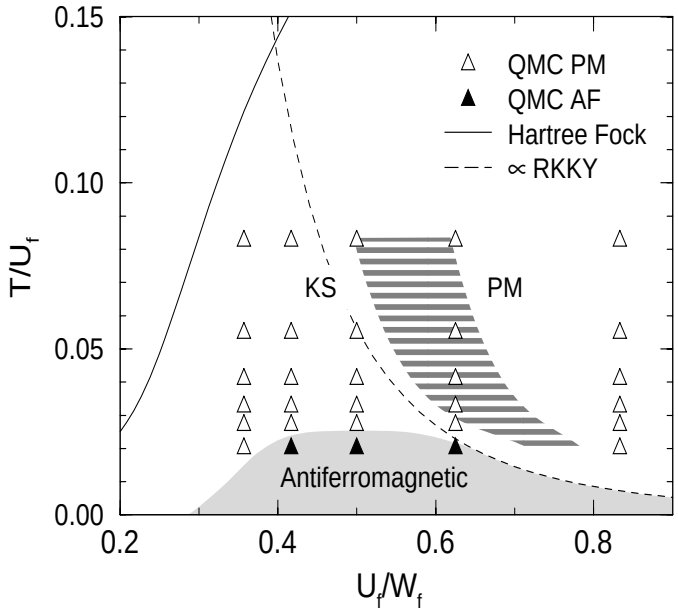

FIG. 4. The magnetic phase diagram of the 3D periodic Anderson model. Open triangles are the paramagnetic phase, while solid triangles are antiferromagnetic (see comment in text). The hatched region shows the region of cross–over to a singlet phase. Also shown are the Hartree–Fock and RKKY results.

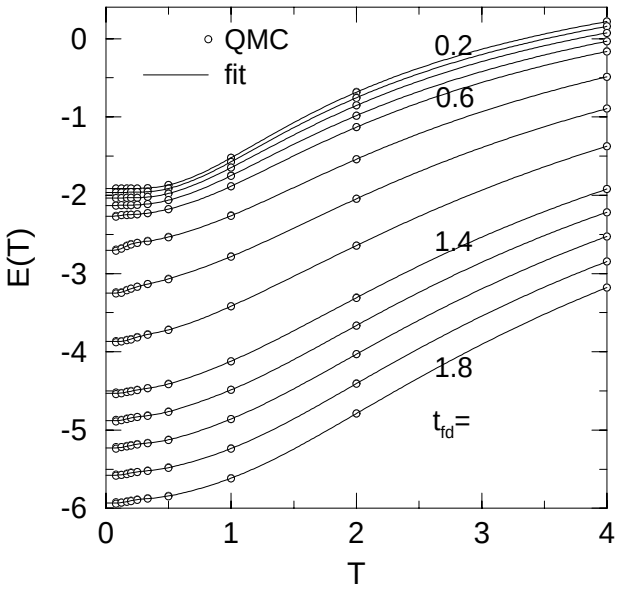

FIG. 5. Energy as a function of temperature. The open circles are the results of QMC simulations. The interpolating lines are the fit described in the text.

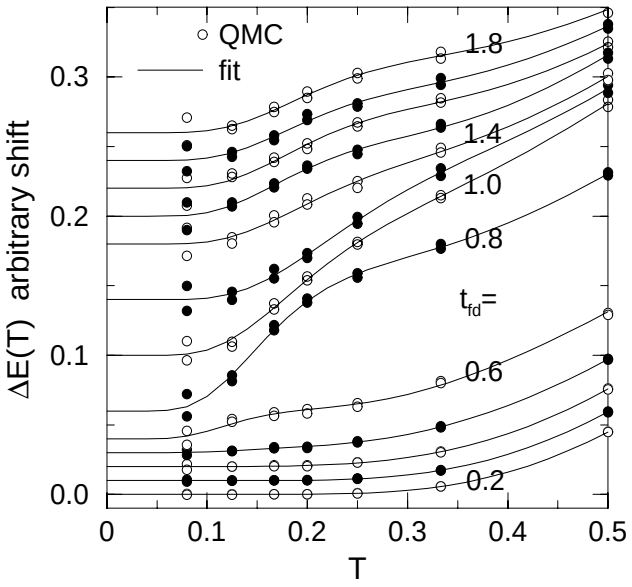

FIG. 6. The data of the preceding figure are reproduced with a higher resolution for the low temperature points to emphasize how the fit tracks the QMC energy data. The doubling of each QMC data point denotes uncertainty in the measured energy. Points on adjacent curves are alternately filled or open.

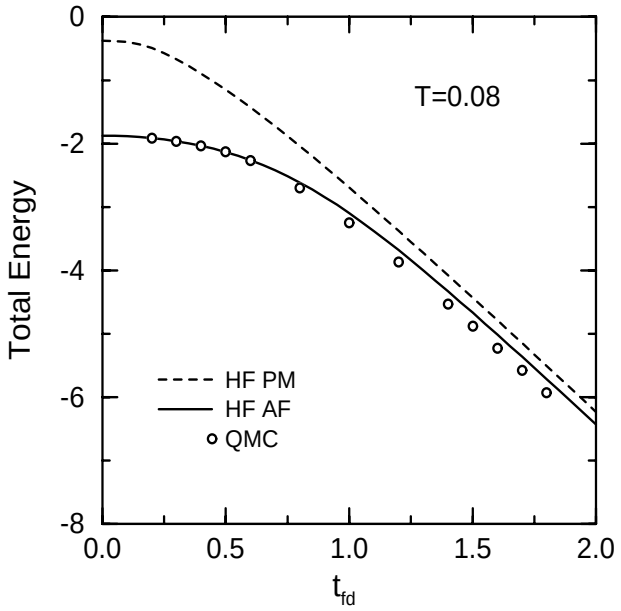

FIG. 7. Hartree–Fock and QMC energies are compared as a function of f–valence hybridization. The dashed curve is the paramagnetic solution, and the solid curve the antiferromagnetic solution. HF is exact at zero hybridization, and shows apparently small deviations at large t_{fd}.

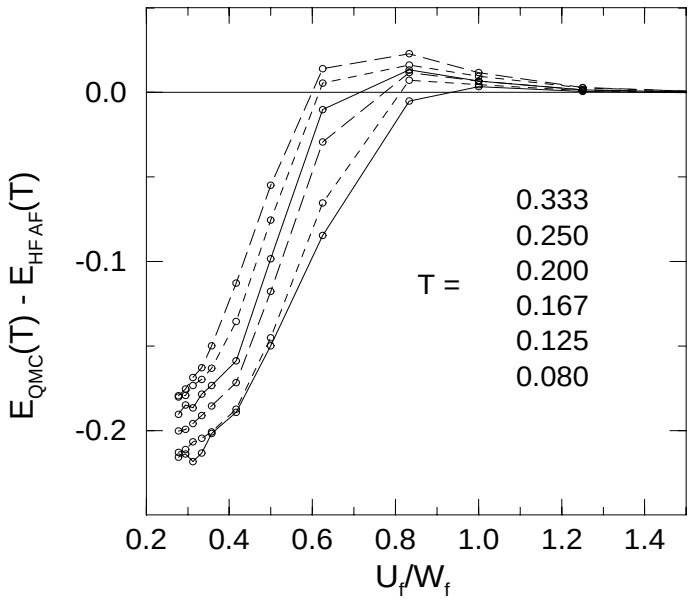

FIG. 8. Difference between antiferromagnetic Hartree-Fock and Quantum Monte Carlo energies. When the ratio U_f/W_f is small, the QMC energies break away rather suddenly and fall below the HF energies.

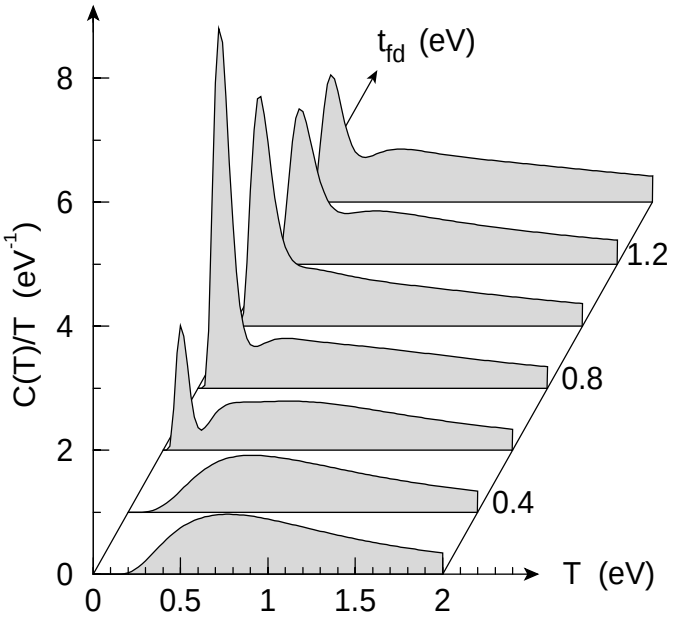

FIG. 9. Specific heat of the PAM for different choices of interband hybridization. The wide structure at $T \sim 1$ is associated with moment formation, while the sharper low T structure is associated with magnetic ordering (either singlet formation or antiferromagnetism). As t_{fd} is decreased, the sharp feature moves to lower temperature and, eventually, is no longer captured by the temperature range accessed in our simulations.

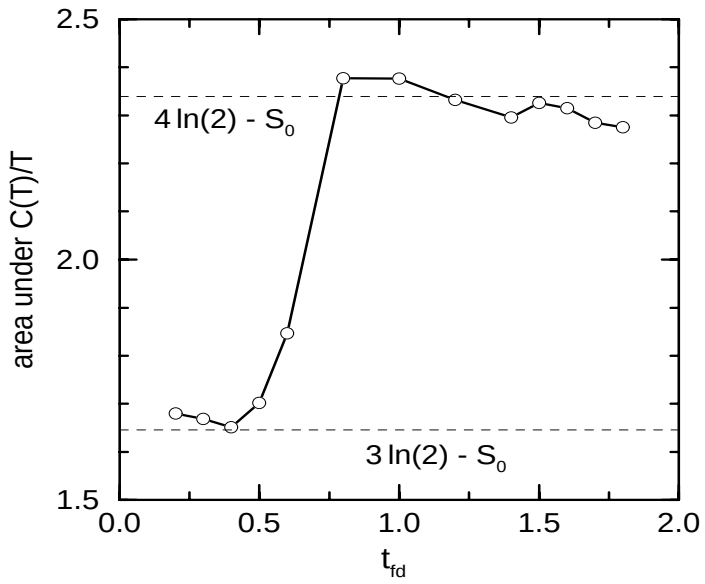

FIG. 10. The integrated areas under the curves of the preceding figure are shown. This measure captures the full entropy $4\ln 2$, adjusted for the effects of the finite lattice, for t_{fd} above 0.75. Below this value there is missing entropy, indicating that there is indeed a peak in C/T at lower temperatures. $S_0 = 0.4332$ for a 4^3-site periodic lattice.

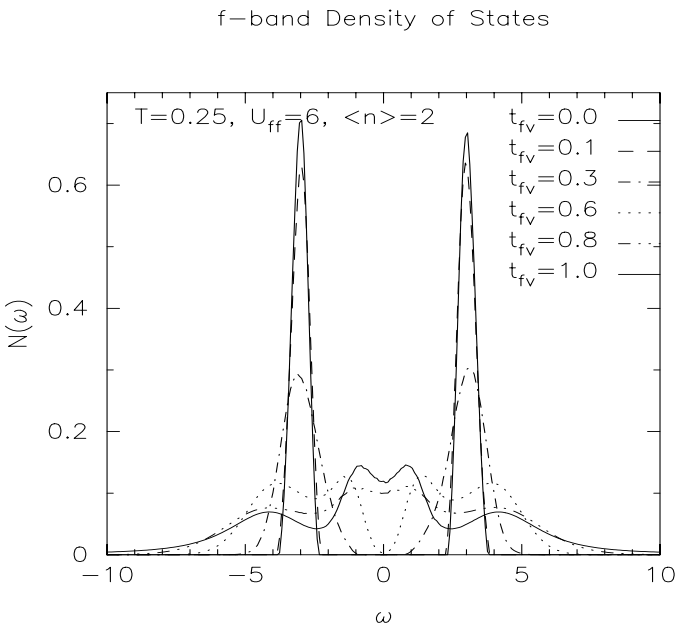

FIG. 11. The f electron density of states for different choices of t_{fd} at $T = t_{dd}/4$. At small t_{fd}, $N_f(\omega)$ consists of the two narrow bands at $\pm U_f/2$ expected for a localized orbital. At larger t_{fd}, $N_f(\omega)$ broadens and develops a Kondo resonance near $\omega = 0$.

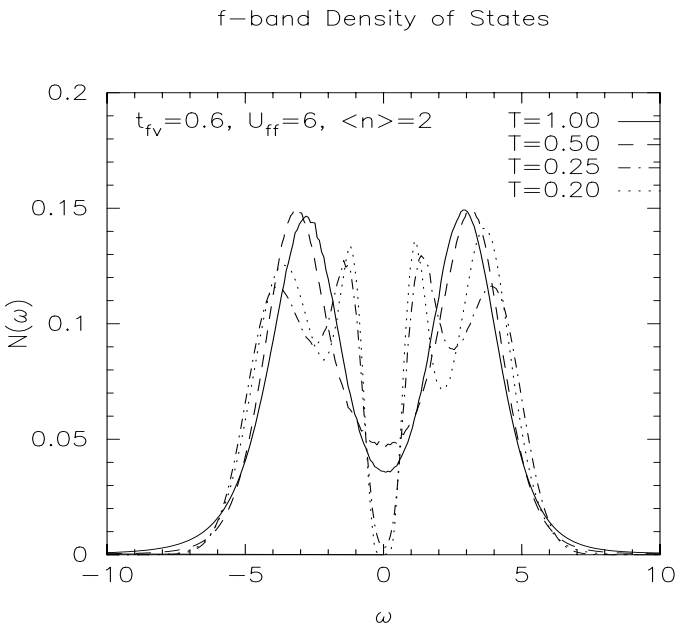

FIG. 12. The f electron density of states for $t_{fd} = 0.6$ at different temperatures. As T is lowered, the broad Mott peaks develop sharper Kondo resonances.

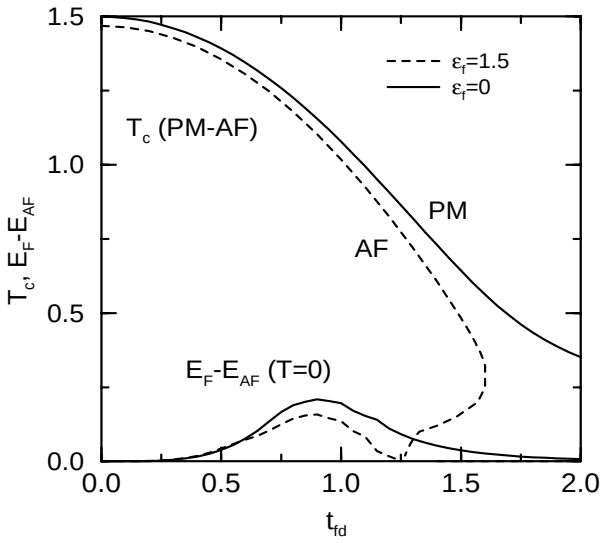

FIG. 13. The Hartree-Fock phase diagram in the non–symmetric limit is compared to the symmetric case. The region of antiferromagnetism is reduced for non–zero ϵ_f. The real HF Néel temperatures is shown (curves labelled T_c), as well as the ferromagnetic–antiferromagnetic energy differences (curves labelled $E_{\rm F} - E_{\rm AF}$). For the symmetric case ($\epsilon_f = 0$), this energy difference is much closer to the actual Néel temperature seen in Fig. 4. The HF calculations were carried out with Brillouin zone sampling corresponding to 12^3 sites, for $t_{dd} = 1$ and $U_f = 6$.